Electronic Supplementary Information

Covalently bonded dendrimer-maghemite nanosystems: nonviral vectors for in vitro gene magnetofection

Blanca González,[1,3] *Eduardo Ruiz-Hernández,*[1,3] *María José Feito,*[2] *Carlos López de Laorden,*[1,3] *Daniel Arcos,*[1,3] *Cecilia Ramírez-Santillán,*[2] *Concepción Matesanz,*[2] *María Teresa Portolés,*[2] *María Vallet-Regí**[1,3]

[1] Departamento de Química Inorgánica y Bioinorgánica, Facultad de Farmacia. Universidad Complutense de Madrid. Plaza de Ramón y Cajal s/n, 28040 Madrid, Spain.

[2] Departamento de Bioquímica, Facultad de Ciencias Químicas. Universidad Complutense de Madrid. Avenida Complutense s/n, 28040 Madrid, Spain.

[3] Networking Research Center on Bioengineering, Biomaterials and Nanomedicine (CIBER-BBN), Spain.

Reagents

The reactions for the synthesis of dendritic precursors (G1-G3) were performed under an inert atmosphere using standard Schlenk techniques. Dichloromethane was dried by standard procedures over phosphorus (V) oxide and distilled immediately prior to use. The dendritic polyamines $DAB(NH_2)_x$ ($x = 4$, 8 and 16) were purchased from Sigma-Aldrich, Inc. ($x = 4$) and from SyMO-Chem BV ($x = 8$ and 16), 3-isocyanatopropyltriethoxysilane and 3-aminopropyltriethoxysilane from ABCR GmbH & Co. KG and iron (III) chloride hexahydrate, iron (II) chloride tetrahydrate and iron (III) nitrate nonahydrate from Sigma-Aldrich Inc. These compounds were used without further purification. Deionized water was further purified by passage through a Milli-Q Advantage A-10 Purification System (Millipore Corporation) to a final resistivity of 18.2 MΩ cm. All other chemicals (nitric acid 65% wt., ammonia 30% wt., absolute ethanol, acetone, etc) were of the best quality commercially available and used as received.

Equipment

Solution state nuclear magnetic resonance (NMR) spectra were recorded on a Bruker AVANCE AV-250 and a Bruker AVANCE AV-500 spectrometers. Chemical shifts are reported in parts per million (δ) with reference to residual solvent resonances.

Electrospray mass spectrometry (ESI MS) analyses were conducted on a “QSTAR Pulsar i” mass spectrometer from Applied Biosystems, equipped with a hybrid analyser Q-TOF (quadrupole-time of flight). The samples were directly infused into the ESI source using a syringe pump at a flow rate of 10 μL/min.

Fourier transformed infrared (FTIR) spectra were colleted in a Thermo Nicolet Nexus spectrometer equipped with a *Goldengate* attenuated total reflectance (ATR) device.

Dynamic light scattering (DLS) and zeta-potential (ζ-potential) measurements were performed in a Zetasizer Nano Series instrument, fitted with a 633 nm laser and coupled to a MPT-2 multipurpose titrator from Malvern. ζ-potential can be described by Smoluchowski's equation: $\zeta = 4\pi\eta U/\varepsilon$, where U is the electrophoretic mobility, η is the viscosity of water, and ε is the dielectric constant of water. Measurements were made using 10 mL of each sample of an iron oxide concentration ranging 1 to 5 mg/mL and the pH was adjusted by titrating with 0.10 M HNO_3 or 0.10 M NH_4OH solutions at 298 K. Each point was taken on triplicate.

Inductively coupled plasma-atomic emission spectroscopy (ICP-AES) analyses were collected in a Varian VISTA AX apparatus. A defined volume of the colloidal samples was digested in $HClO_4$, then in HF and H_2SO_4 and, finally, in concentrated HCl before the measurements. The obtained iron concentration was translated into γ-Fe_2O_3, since no other iron oxide phase was observed in the X-ray diffraction analysis of dry powdered samples.

X-ray powder diffraction (XRD) data were collected on a Philips X'Pert Plus diffractometer (Philips Electronics NV, Eindhoven, Netherlands) with Bragg-Brentano geometry, operating with CuKα radiation (λ = 1.5406 Å) at 40 kV and 20 mA. The diffractograms were collected over the range between 5° and 120° 2θ with a step size of 0.02° and a contact time of 10 s per step.

The magnetic characterization system used was a LakeShore (7304 model) Vibrating Sample Magnetometer. The hysteresis of the magnetization of the ferrofluids was obtained by changing H between + 12500 and – 12500 Oe at 298 K.

Chemical microanalyses were performed with a Perkin Elmer 2400 CHN thermo analyzer. Thermogravimetric analysis (TGA) and differential thermal analysis (DTA) were carried out in air between 30 and 1000 °C with a flow rate of 100 mL/min and a heating rate of 5 °C/min using a Perkin Elmer Pyris Diamond thermobalance.

Gene delivery experiments were carried out in the presence and in the absence of a magnetic field provided by a magnetic plate (MF14000, OzBiosciences).

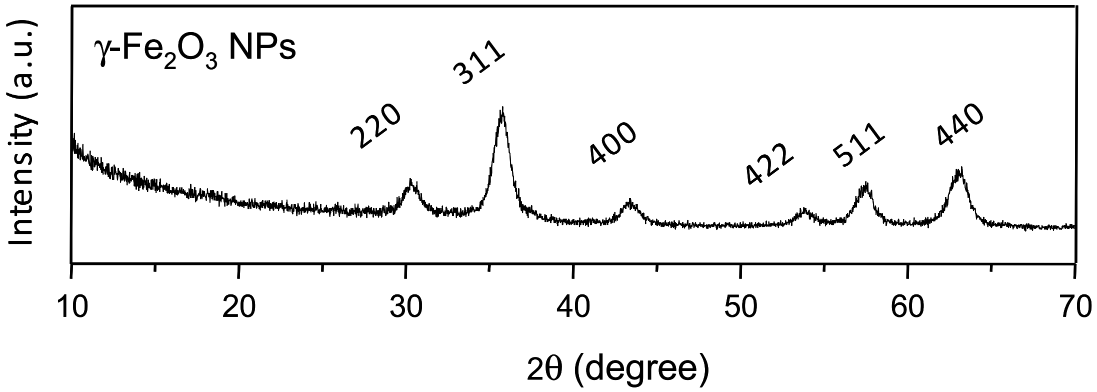

Figure S1. X-ray powder diffraction pattern of the γ-Fe_2O_3 NPs.

Selected characterization data for ***G1***:

δ_{H}(500 MHz; $\mathrm{CDCl_3}$) 5.86 (0.35H, t, N*H*CONH), 5.68 (0.65H, t, N*H*CONH), 5.56 (0.35H, t, N*H*CONH), 5.39 (0.65H, t, N*H*CONH), 3.65 (6H, q, $\mathrm{CH_3C}\mathit{H_2}\mathrm{O}$), 3.04 (2H, m, $\mathrm{C}\mathit{H_2}\mathrm{NHCONH}$), 2.98 (2H, m, $\mathrm{C}\mathit{H_2}\mathrm{NHCONH}$), 2.58 (6H, m, $\mathrm{C}\mathit{H_2}\mathrm{NH_2}$), 2.30 (8H, br, $\mathrm{C}\mathit{H_2}\mathrm{N}$), 2.24 (4H, br, $\mathrm{C}\mathit{H_2}\mathrm{N}$), 1.55 (6H, br, $\mathrm{N}\mathit{H_2}$), 1.44 (10H, m, $\mathrm{CH_2C}\mathit{H_2}\mathrm{CH_2}$), 1.27 (4H, br, $\mathrm{CH_2C}\mathit{H_2}\mathrm{C}\mathit{H_2}\mathrm{CH_2}$), 1.06 (9H, t, $\mathrm{C}\mathit{H_3}\mathrm{CH_2O}$), 0.47 (2H, t, $\mathrm{C}\mathit{H_2}\mathrm{Si}$).

δ_{C}(125.77 MHz; $\mathrm{CDCl_3}$): 158.6 (NH*C*ONH), 58.0 ($\mathrm{CH_3}\mathit{C}\mathrm{H_2O}$), 53.7, 51.7 ($\mathit{C}\mathrm{H_2N}$), 42.6 ($\mathit{C}\mathrm{H_2NHCONH}$), 40.5 ($\mathit{C}\mathrm{H_2NH_2}$), 38.8 ($\mathit{C}\mathrm{H_2NHCONH}$), 30.6, 30.5, 29.9, 24.8, 24.7, 24.5 ($\mathrm{CH_2}\mathit{C}\mathrm{H_2CH_2}$), 27.0, 23.5 ($\mathrm{CH_2}\mathit{C}\mathrm{H_2}\mathit{C}\mathrm{H_2CH_2}$, $\mathrm{NCH_2}\mathit{C}\mathrm{H_2CH_2Si}$), 18.0 ($\mathit{C}\mathrm{H_3CH_2O}$), 7.4 ($\mathit{C}\mathrm{H_2Si}$).

δ_{Si}(99.4 MHz; $\mathrm{CDCl_3}$): -45.4 (s, $\mathrm{CH_2}\mathit{Si}\mathrm{(OCH_2CH_3)_3}$).

ν_{max}(ATR)/$\mathrm{cm^{-1}}$ 3347 ν(NH) NHCONH; 3285 ν(NH) $\mathrm{NH_2}$; 2926, 2863, 2799 ν_{as}(CH), ν_{s}(CH) $\mathrm{CH_2}$ and $\mathrm{CH_3}$ groups; 1639 ν(C=O) amide I; 1564 δ(CNH) amide II; 1462, 1388 ν(CN); 1250 ν(CN) + δ(CNH) amide III; 1100, 1073 ν_{as}(SiO), 953 ν_{s}(SiO), 770 δ(SiOC) SiOC group; 639 ν(SiC).

Selected characterization data for ***G2***:

δ_{H}(500 MHz; $\mathrm{CDCl_3}$) 5.45 (br, N*H*CONH), 5.40 (br, N*H*CONH), 5.32 (br, N*H*CONH), 5.27 (br, N*H*CONH), 3.65 (6H, q, $\mathrm{CH_3C}\mathit{H_2}\mathrm{O}$), 2.67 (2H, br, $\mathrm{C}\mathit{H_2}\mathrm{NHCONH}$), 2.62 (2H, m, $\mathrm{C}\mathit{H_2}\mathrm{NHCONH}$), 2.22 (14H, t, $\mathrm{C}\mathit{H_2}\mathrm{NH_2}$), 1.97 (22H, t, $\mathrm{C}\mathit{H_2}\mathrm{N}$), 1.94 (14H, br, $\mathrm{C}\mathit{H_2}\mathrm{N}$), 1.25 (14H, s, $\mathrm{N}\mathit{H_2}$), 1.09 (26H, m, $\mathrm{CH_2C}\mathit{H_2}\mathrm{CH_2}$), 0.90 (4H, br, $\mathrm{CH_2C}\mathit{H_2}\mathrm{C}\mathit{H_2}\mathrm{CH_2}$), 0.72 (9H, t, $\mathrm{C}\mathit{H_3}\mathrm{CH_2O}$), 0.11 (2H, t, $\mathrm{C}\mathit{H_2}\mathrm{Si}$).

δ_{C}(125.77 MHz; $\mathrm{CDCl_3}$) 159.0 (NH*C*ONH), 58.3 ($\mathrm{CH_3}\mathit{C}\mathrm{H_2O}$), 53.7, 52.3, 51.9, 51.7 ($\mathit{C}\mathrm{H_2N}$), 42.8 ($\mathit{C}\mathrm{H_2NHCONH}$), 40.7 ($\mathit{C}\mathrm{H_2NH_2}$), 38.7 ($\mathit{C}\mathrm{H_2NHCONH}$), 30.9, 27.5, 24.7 ($\mathrm{CH_2}\mathit{C}\mathrm{H_2CH_2}$), 25.1, 23.8 ($\mathrm{CH_2}\mathit{C}\mathrm{H_2}\mathit{C}\mathrm{H_2CH_2}$, $\mathrm{NCH_2}\mathit{C}\mathrm{H_2CH_2Si}$), 18.3 ($\mathit{C}\mathrm{H_3CH_2O}$), 7.7 ($\mathit{C}\mathrm{H_2Si}$).

δ_{Si}(99.4 MHz; $\mathrm{CDCl_3}$) -45.7 (s, $\mathrm{CH_2}\mathit{Si}\mathrm{(OCH_2CH_3)_3}$).

Selected characterization data for ***G3***:

δ_{H}(500 MHz; $\mathrm{CDCl_3}$) 5.43 (br, N*H*CONH), 5.17 (br, N*H*CONH), 3.52 (6H, q, $\mathrm{CH_3C}\mathit{H_2}\mathrm{O}$), 2.89 (4H, br, $\mathrm{C}\mathit{H_2}\mathrm{NHCONH}$), 2.44 (30H, br, $\mathrm{C}\mathit{H_2}\mathrm{NH_2}$), 2.16 (84H, br, $\mathrm{C}\mathit{H_2}\mathrm{N}$), 1.48 (30H, br, $\mathrm{N}\mathit{H_2}$), 1.30 (58H, br, $\mathrm{CH_2C}\mathit{H_2}\mathrm{CH_2}$), 1.11 (4H, br, $\mathrm{CH_2C}\mathit{H_2}\mathrm{C}\mathit{H_2}\mathrm{CH_2}$), 0.93 (9H, t, $\mathrm{C}\mathit{H_3}\mathrm{CH_2O}$), 0.34 (2H, t, $\mathrm{C}\mathit{H_2}\mathrm{Si}$).

δ_{C}(125.77 MHz; $\mathrm{CDCl_3}$) 158.2 (NH*C*ONH), 57.7 ($\mathrm{CH_3}\mathit{C}\mathrm{H_2O}$), 53.7, 53.0, 51.7, 51.6, 51.3 ($\mathit{C}\mathrm{H_2N}$), 42.3 ($\mathrm{C}\mathit{H_2}\mathrm{NHCONH}$), 40.1 ($\mathit{C}\mathrm{H_2NH_2}$), 38.2 ($\mathit{C}\mathrm{H_2NHCONH}$), 30.2, 24.5, 23.9 ($\mathrm{CH_2}\mathit{C}\mathrm{H_2CH_2}$), 26.9, 23.2 ($\mathrm{CH_2}\mathit{C}\mathrm{H_2}\mathit{C}\mathrm{H_2CH_2}$, $\mathrm{NCH_2}\mathit{C}\mathrm{H_2CH_2Si}$), 17.7 ($\mathit{C}\mathrm{H_3CH_2O}$), 7.1 ($\mathit{C}\mathrm{H_2Si}$).

δ_{Si}(99.4 MHz; $\mathrm{CDCl_3}$) -45.4 (s, $\mathrm{CH_2}\mathit{Si}\mathrm{(OCH_2CH_3)_3}$).

Table S1. Data and assignments of ESI-TOF mass spectra of dendritic precursors **G1**-**G3**.

m/z experimental (amu)	Relative abundance (%)	Assignment	m/z theoretical (amu)	Δm/z (amu)
		Dendritic precursor **G1** [a]		
317.34	24.14	$[M_0 + H^+]^+$	317.34	
564.47	100	$[M_1 + H^+]^+$	564.46	247.13
811.59	11.23	$[M_2 + H^+]^+$	811.59	247.12
1058.71	0.36	$[M_3 + H^+]^+$	1058.71	247.12
159.18	9.83	$[M_0 + 2H^+]^{2+}$	159.17	
282.74	20.77	$[M_1 + 2H^+]^{2+}$	282.73	123.56
406.30	20.49	$[M_2 + 2H^+]^{2+}$	406.30	123.56
		Dendritic precursor **G2** [b]		
387.42	28.49	$[M_0 + 2H^+]^{2+}$	387.40	
510.98	100	$[M_1 + 2H^+]^{2+}$	510.97	123.56
634.55	39.73	$[M_2 + 2H^+]^{2+}$	634.53	123.57
758.62	6.99	$[M_3 + 2H^+]^{2+}$	758.59	123.57
		Dendritic precursor **G3** [c]		
844.40	27.59	$[M_0 + 2H^+]^{2+}$	844.37	
967.97	47.34	$[M_1 + 2H^+]^{2+}$	967.93	123.57
1091.53	22.72	$[M_2 + 2H^+]^{2+}$	1091.49	123.56
1215.10	5.14	$[M_3 + 2H^+]^{2+}$	1215.05	123.57
1338.66	0.70	$[M_4 + 2H^+]^{2+}$	1338.62	123.56
563.28	55.99	$[M_0 + 3H^+]^{3+}$	563.25	
645.65	100	$[M_1 + 3H^+]^{3+}$	645.62	82.37
728.03	58.70	$[M_2 + 3H^+]^{3+}$	728.00	82.38
810.41	15.96	$[M_3 + 3H^+]^{3+}$	810.37	82.38
422.71	17.85	$[M_0 + 4H^+]^{4+}$	422.69	
484.50	63.84	$[M_1 + 4H^+]^{4+}$	484.49	61.79
546.28	35.16	$[M_2 + 4H^+]^{4+}$	546.25	61.78
608.07	9.48	$[M_3 + 4H^+]^{4+}$	608.03	61.79

[a] M_0 = DAB$(NH_2)_4$ = $C_{16}H_{40}N_6$; M_1 = DAB$(NH_2)_3Si_1$ = $C_{26}H_{61}N_7O_4Si$; M_2 = DAB$(NH_2)_2Si_2$ = $C_{36}H_{82}N_8O_8Si_2$; M_3 = DAB$(NH_2)_1Si_3$ = $C_{46}H_{103}N_9O_{12}Si_3$.

[b] M_0 = DAB$(NH_2)_8$ = $C_{40}H_{96}N_{14}$; M_1 = DAB$(NH_2)_7Si_1$ = $C_{50}H_{117}N_{15}O_4Si$; M_2 = DAB$(NH_2)_6Si_2$ = $C_{60}H_{138}N_{16}O_8Si_2$; M_3 = DAB$(NH_2)_5Si_3$ = $C_{70}H_{159}N_{17}O_{12}Si_3$.

[c] M_0 = DAB$(NH_2)_{16}$ = $C_{88}H_{208}N_{30}$; M_1 = DAB$(NH_2)_{15}Si_1$ = $C_{98}H_{229}N_{31}O_4Si$; M_2 = DAB$(NH_2)_{14}Si_2$ = $C_{108}H_{250}N_{32}O_8Si_2$; M_3 = DAB$(NH_2)_{13}Si_3$ = $C_{118}H_{271}N_{33}O_{12}Si_3$; M_4 = DAB$(NH_2)_{12}Si_4$ = $C_{128}H_{292}N_{34}O_{16}Si_4$.

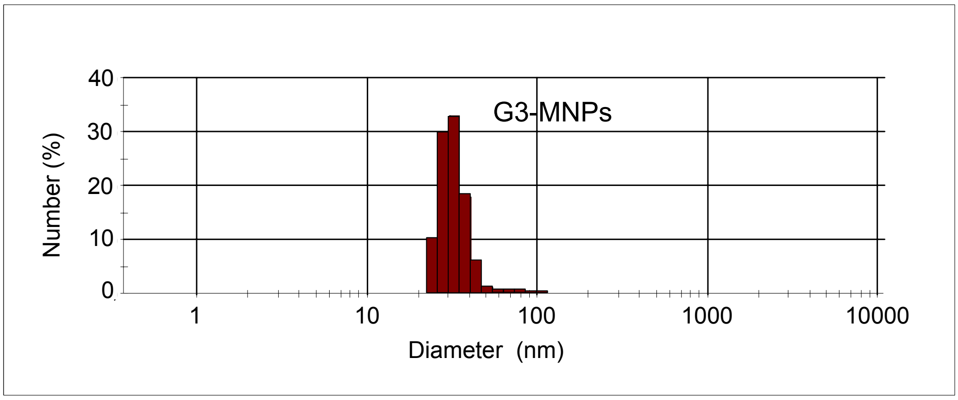

Figure S2. Number weighted hydrodynamic diameter distribution obtained by DLS for the **G3** dendrimer functionalized MNPs nanoparticles in water (*ca.* 1-5 mg/mL) at pH 7.4, measured after seven months of storage. Mean hydrodynamic diameter *ca.* 36 nm.